Eur. Phys. J. D **22**, 65–73 (2003)
DOI: 10.1140/epjd/e2002-00212-2

THE EUROPEAN PHYSICAL JOURNAL D

NMR study of the dissolution of laser-polarized xenon

P. Berthault and H. Desvaux[a]

Laboratoire Commun de RMN, DSM/DRECAM/Service de Chimie Moléculaire[b], CEA/Saclay, 91191 Gif-sur-Yvette, France

Received 29 April 2002 / Received in final form 26 July 2002
Published online 22 October 2002 –

Abstract. NMR of laser-polarized xenon is used to probe the dissolution behaviour of the noble gas in different liquids. The dissolution and self-relaxation rates are extracted *via* a macroscopic model, and comparison of the decay rate of the xenon magnetization in deuterated and non-deuterated solvent pairs allows the determination of the pure dipole-dipole contribution to relaxation. A transient convective effect, tentatively assigned to the xenon concentration gradient, is observed and characterized by diffusion encoding MRI experiments. The flow of xenon penetrates inside the solvent near the walls of the NMR tube, the longitudinal images showing a "⋂" shape, the transverse ones a "O" shape. This convection effect has implications for delivery conditions of laser-polarized xenon in continuous flow experiments and magnetic resonance imaging.

PACS. 32.80.Bx Level crossing and optical pumping – 76.60.-k Nuclear magnetic resonance and relaxation – 76.60.Pc NMR imaging – 82.56.Lz Diffusion – 82.40.Ck Pattern formation in reactions with diffusion, flow and heat transfer

1 Introduction

NMR represents a powerful tool to obtain structural and dynamic data at the atomic scale, but even with the strongest magnets today available, it still suffers at room temperature from low sensitivity due to the small couplings between the nuclear magnetic moments and the magnetic field. The nuclear polarization can however be enhanced by several orders of magnitude by resorting to optical pumping [1]. The target compounds of such methods are noble gases of nuclear spin 1/2 (^{129}Xe and ^{3}He), as their longitudinal self-relaxation can be as long as several hours [2,3]. Recently, it has been shown that the use of laser-polarized xenon which has a much larger solubility in the most common liquids than helium, could afford polarization enhancement *via* through-space dipole-dipole cross-relaxation to other nuclear spins [4]. Two approaches were further explored: selective polarization transfer was measured in order to locate xenon inside hydrophobic cavities [5–9]; also non selective polarization transfer was considered [4,10] in order to improve the NMR signal of other nuclei. In any case, the poor values of the intermolecular relaxation rates, the transient character of the noble gas magnetization and the limited xenon solubility impede significant gain in sensitivity. To circumvent the last difficulty, resorting to laser-polarized liquid [11] or supercritical [12,13] xenon has been suggested. However the transient nature of the xenon magnetization remains an obstacle to multidimensional NMR experiments, and the only solution consists of reaching a steady-state by using a continuous flow of laser-polarized gas [14–17]. This solution has not yet been reported for liquid-state application, but in an effort to reach it, we feel it is important to take advantage of the availability of laser-polarized xenon to follow transient events during the dissolution of the gas, in a procedure close to that used by Navon *et al.* [4]. Our study (i) reveals the presence, during the dissolution step of xenon, of a transient convective phenomenon, characterized by MRI; and (ii) allows the evaluation of the solvent contribution to xenon spin relaxation through dipolar interactions by comparison of the xenon magnetization decay in deuterated and non-deuterated solvents.

2 Experimental

2.1 Experimental protocol

To study the dissolution and relaxation of xenon in deuterated and non-deuterated solvents, the following protocol is systematically used.

1. A 5 mm o.d. NMR tube **a** (4.2 mm i.d.) closed by a screw cap and containing 500 microliters of solvent[1] is first degassed by several freeze-pump-thaw cycles and thermalized inside the superconducting magnet.

[a] e-mail: hdesvaux@cea.fr
[b] URA CNRS/CEA 331

[1] From Eurisotop for the deuterated solvents and from Aldrich for the others (analytical grade).

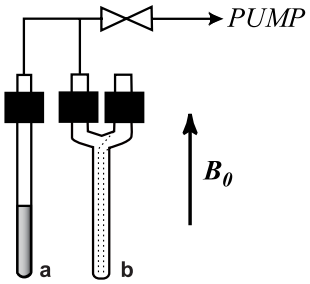

Fig. 1. Scheme of the Joule – Gay Lussac expansion from the modified NMR tube **b** to the NMR tube **a** which contains the degassed solvent. This operation is performed in the fringe field of the NMR magnet.

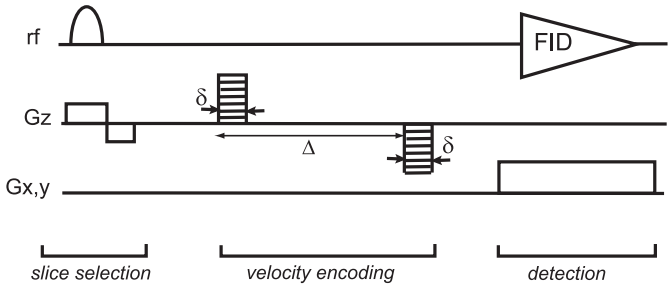

Fig. 2. Pulse sequence used for 2D velocimetry experiments. The soft pulse combined with a pulsed field gradient to select a slice along z has a Gaussian shape and a duration of 5 ms (flip angle of $\sim 10°$). The gradient strength value is 5×10^{-3} Tm^{-1}, corresponding to a slice depth of about 0.5 cm. 16 gradient values are used in the ramp from 0 to 0.2 Tm^{-1} to create the second dimension.

2. Xenon is polarized by the spin exchange method [18] using an home-built apparatus allowing the preparation of samples with a nuclear polarization of about 15% [7]. After each cycle of optical pumping (∼10 min), laser-polarized xenon is condensed (and thus separated from gaseous nitrogen) into a modified NMR tube **b** (Fig. 1) which fits inside a solenoid producing a 5 kG magnetic field, everything being immersed in a bath of liquid nitrogen.
3. The tube **b** and the solenoid are moved to the fringe field of the spectrometer magnet and the tube is warmed up.
4. The gaseous laser-polarized xenon contained in **b** is expanded into the NMR tube **a** using a vacuum line through a classical Joule – Gay Lussac expansion (Fig. 1). After one cycle of optical pumping and expansion, the tube **a** is filled by ∼0.4 bar of pure xenon.
5. The tube **a** is quickly put back inside the superconductive magnet. The typical duration of this transfer operation is ∼20 s, and as checked by monitoring the xenon chemical shift, no important temperature variation of the solution occurs.
6. The NMR experiment starts.

Most of the experiments are performed at 290 K on a DRX500 Bruker narrow bore spectrometer (11.7 T) equipped with a 5 mm Nalorac direct broadband probehead with three axes field gradients. The top of the detection coils is located ∼10 mm below the gas-liquid interface. The gas to solvent volume ratio in tubes **a** is about 4.

2.2 NMR experiments

The first series of experiments consists in single 1D xenon spectra separated by definite time intervals, in order to follow the appearance of the dissolved gas. The acquisitions, made of one scan with a small flip angle (<5°), are separated by delays varying from 30 s to 4 min, in order to sample correctly the dynamic processes without altering too much the out-of-equilibrium xenon magnetization.

Dynamic imaging of the xenon flow inside the solvent is performed at 290 K using the three axes gradient capabilities of our probehead. Due to possible xenon radiation damping effects [19], in all sequences, only gradient echos are applied without 180° refocusing pulses. Because of the fast evolution of the xenon motions during the dissolution step and also in order to limit the experiment times, only 2D experiments acquired in about 15 s are performed[2].

For measuring the xenon velocity along the vertical (z) axis of the NMR tube, we use a sequence initially proposed by Callaghan and Xia [21] and adapted recently for laser-polarized xenon for studying edge-enhancement by diffusion [22] or convection in the gas phase above liquid polarized xenon [23]. In this sequence (Fig. 2), a soft pulse of Gaussian shape combined with a pulsed field gradient along z selects an horizontal slice of about 5 mm (size measured in a 1D experiment). The two following field gradient ramps serve to encode the velocity of dissolved xenon atoms. The field gradient applied during the acquisition codes in frequency, and therefore allows the observation of the z-velocity distribution along x or y. Each 2D map thus contains, in the indirect dimension, information about the diffusion rate (through the linewidth) and the velocity (the shift relative to the zero frequency). Home-written C software allows the numerical processing of these experiments. To estimate the translational diffusion coefficient D and the group velocity v, we have assumed that the Fourier Transform of the signal in the indirect dimension $s(Z)$ is a shifted Gaussian [21]. The extraction of D and v is obtained by a non linear least-square fitting of $s(Z)$ to the equation:

$$s(Z) = \frac{1}{\sqrt{4\pi D \Delta_{\mathrm{eff}}}} \exp\left[-\frac{(Z - v\Delta)^2}{4D\Delta_{\mathrm{eff}}}\right] \qquad (1)$$

with Δ the delay between the two encoding gradients and $\Delta_{\mathrm{eff}} = \Delta - \delta/3$ the effective migration time, which takes into account the duration δ of the gradients.

Longitudinal and slice-selected transverse images of the xenon inside the NMR tube during the dissolution and relaxation steps are obtained using the FLASH sequence [24,25], which consists of a small flip-angle pulse, followed by a phase encoding gradient applied along a

[2] Echo Planar Imaging [20] could not be employed due to technical limitations of our liquid-state NMR spectrometer.

direction, and detection in the presence of a frequency encoding gradient applied along a second direction. In the transverse image, a slice of 5 mm is selected by replacement of the small hard pulse by a soft pulse of sinc shape combined with a field gradient applied along the third (z) direction.

3 Results

3.1 Macroscopic model for dissolution and relaxation of laser-polarized xenon

The dissolution of laser-polarized xenon into an evacuated solvent followed by liquid state NMR is a phenomenon both time- and space-dependent. Indeed the xenon magnetization in the gaseous phase relaxes slowly towards its equilibrium value with a relaxation time T_1^{g} (on the order of 120 minutes at ambient temperature [7]), while the xenon in the liquid state relaxes with a much shorter relaxation time T_1^{l}. The two phases are connected by the exchange of xenon at the interface. At the beginning, a flow of xenon from the gas towards the solution takes place due to the concentration gradient. But even when the equilibrium is reached, by diffusion and convection the system still exchanges magnetization between the two phases. We consequently expect the presence not only of a gradient of concentration but also of a gradient of polarization along the sample from the surface of the liquid to the bottom of the NMR tube. The difficulties to analytically treat the system at a microscopic scale, mainly because it requires the perfect knowledge of all transport mechanisms, lead us to consider a simpler macroscopic model, which fits relatively well all experimental results. It essentially treats the properties of xenon dissolution by considering the xenon magnetization inside the detection coil as uniform, disregarding any concentration and polarization gradient. The connection between this phenomenological model and the observed transient convection is discussed in Section 3.5.

Since the system is out of chemical equilibrium at the beginning, assuming that the dissolution can be considered as a first rank reaction, the number of xenon atoms $n(t)$ in the liquid phase is:

$$n(t) = n_\infty(1 - \mathrm{e}^{-k_{\mathrm{solv}}t}) \tag{2}$$

where k_{solv} is the dissolution rate and n_∞ is related to the final density of xenon. The variation of the dissolved xenon magnetization S_z can be written:

$$\frac{\mathrm{d}}{\mathrm{d}t}S_z = P_{\mathrm{g}}\frac{\mathrm{d}}{\mathrm{d}t}n(t) - \frac{S_z}{T_1^{\mathrm{l}}} + k_{\mathrm{diff}}n_\infty P_{\mathrm{g}} - k_{\mathrm{diff}}S_z. \tag{3}$$

The successive terms on the right side of equation (3) are the dissolution of xenon from the gaseous phase whose polarization is P_{g}, the longitudinal relaxation of the dissolved xenon and then the diffusion of the xenon from and towards the gaseous phase. Due to the enhancement factor resulting from optical pumping, the terms depending upon the xenon magnetization at thermal equilibrium can be discarded. The diffusion represents the exchange between the two phases, when concentration is equilibrated, *i.e.* when convection (see below) has disappeared. In these conditions, the expression of $n(t)$ is valid for $t \gg 1/k_{\mathrm{solv}}$. The variation of the gaseous polarization is:

$$\frac{\mathrm{d}}{\mathrm{d}t}P_{\mathrm{g}} = -\frac{P_{\mathrm{g}}}{T_1^{\mathrm{g}}} + k_{\mathrm{diff}}\frac{n_\infty}{n_0}(P_{\mathrm{l}} - P_{\mathrm{g}}) \tag{4}$$

where n_0 is the number of xenon atoms in the gaseous phase at concentration equilibrium. Assuming $T_1^{\mathrm{l}} \ll T_1^{\mathrm{g}}$:

$$P_{\mathrm{g}} = P_{\mathrm{g}}^0 \exp\left(-t\left(\frac{1}{T_1^{\mathrm{g}}} + \frac{n_\infty}{n_0}k_{\mathrm{diff}}\right)\right). \tag{5}$$

Equation (3) can then be integrated, with the initial condition $S_z = 0$ at $t = 0$:

$$S_z = A\left(\mathrm{e}^{-\lambda_1 t} - \mathrm{e}^{-\lambda_2 t}\right) + B\left(\mathrm{e}^{-\lambda_3 t} - \mathrm{e}^{-\lambda_2 t}\right) \tag{6}$$

with:

$$\lambda_1 = k_{\mathrm{solv}} + \frac{1}{T_1^{\mathrm{g}}} + \frac{n_\infty}{n_0}k_{\mathrm{diff}} \tag{7}$$

$$\lambda_2 = \frac{1}{T_1^{\mathrm{l}}} + k_{\mathrm{diff}} \tag{8}$$

$$\lambda_3 = \frac{1}{T_1^{\mathrm{g}}} + \frac{n_\infty}{n_0}k_{\mathrm{diff}} \tag{9}$$

$$A = P_{\mathrm{g}}^0 k_{\mathrm{solv}}\, n_\infty/(\lambda_2 - \lambda_1) \tag{10}$$

$$B = P_{\mathrm{g}}^0 k_{\mathrm{diff}}\, n_\infty/(\lambda_2 - \lambda_3). \tag{11}$$

The different characteristic rates can be expressed as:

$$k_{\mathrm{diff}} = B(\lambda_2 - \lambda_3)(\lambda_1 - \lambda_3)/A(\lambda_1 - \lambda_2) \tag{12}$$

$$\frac{1}{T_1^{\mathrm{l}}} = \lambda_2 - k_{\mathrm{diff}} \tag{13}$$

$$k_{\mathrm{solv}} = \lambda_1 - \lambda_3 \simeq \lambda_1 \tag{14}$$

$$\frac{1}{T_1^{\mathrm{g}}} = \lambda_3 - k_{\mathrm{diff}}\, n_\infty/n_0 \simeq \lambda_3 \tag{15}$$

where we have assumed for equation (14) that the relaxation of the gas is much slower than the dissolution, and for equation (15) that because of the molar fraction of dissolved xenon and the gas to solvent volume ratio, the term $k_{\mathrm{diff}}n_\infty/n_0$ is negligible [26].

In equation (6), t may have to be replaced by $t - t_0$ where t_0 represents the positive or negative dead-time corresponding to the delay for migration from the interface towards the detection coil minus the elapsed time between the expansion of the polarized gas into the NMR tube and the beginning of the acquisition. We do not consider, even if an analytical solution exists, the effect of the read pulses on the xenon magnetization evolution. Indeed the experimental determination of the consequent signal loss cannot be accurately performed, as it depends on the ratio of the liquid volume to the volume covered by the NMR coils and on the exact value of the pulse flip angle. The numerical determination of this attenuation factor during the fitting

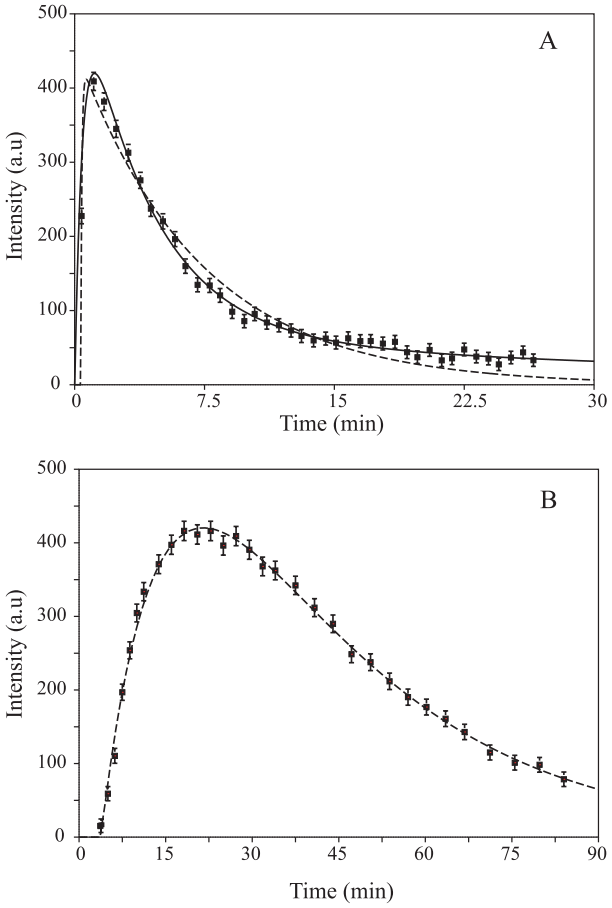

Fig. 3. Evolution of the xenon signal during dissolution in (A) trifluoroethanol-d3 (CF_3CD_2OD), (B) dichloromethane-d2 (CD_2Cl_2). Temperature: 290 K. Flip angle of the pulse: 4.5°. The best-fit curve to equation (6) is superimposed as a solid line. The dotted line is the best-fit curve with $k_{\rm diff} = 0$. The time scale of the two graphs being different, the time of appearance (dead-time t_0), the dissolution, the relaxation and the behavior for long mixing times (two time constants for the decay of the intensity in the case of trifluoroethanol) strongly differ for these two solvents.

procedure is unstable, since its discrimination from an exponential decay would require high precision and non constant time intervals between xenon signal measurements. The extracted $T_1^{\rm l}$ values are consequently slightly underestimated.

The term proportional to B represents the effect of the diffusion of xenon between the solution and the gaseous phase, when the concentration equilibrium is reached. This term is consequently expected to be small relative to the term proportional to A which represents the effect of starting the experiment out of equilibrium. As observed experimentally, for particular solvents, the slow apparent longitudinal self-relaxation of dissolved xenon makes it impossible to distinguish these two time domains. In these conditions the effect of diffusion is neglected and $k_{\rm diff}$ is taken equal to 0. Equation (6) becomes dependent only on two rates λ_1 and λ_2.

Table 1. Dissolution rates $k_{\rm solv}$ and self-relaxation time $T_1^{\rm l}$ as extracted by fitting to equation (6), the time dependence of laser-polarized xenon signal with considering a diffusion constant $k_{\rm diff}$. The proton dipolar contribution to relaxation $T_{1\rm DD}$ and its relative contribution %DD are extracted by comparing $T_1^{\rm l}$ values in non-deuterated and deuterated solvents and neglecting the ^{2}H dipolar contribution to xenon relaxation relative to the ^{1}H one. For non-deuterated n-hexanol the signal to noise ratio is not sufficient to enable a reliable extraction of the rates.

Solvent	$k_{\rm solv}$ ($\rm min^{-1}$)	$T_1^{\rm l}$ (min)	$T_{1\rm DD}$ (min)	%DD
C_6D_6	0.86	10.8	5.18	68
C_6H_6		3.5		
C_6D_{12}	0.98	10.3	3.48	75
C_6H_{12}		2.6		
CF_3CD_2OD	2.28	4.5	18.02	19
CF_3CD_2OH		3.6	5.66	54
CF_3CH_2OH		2.2		
$C_6D_{13}OD$	0.37	4.3	-	-

3.2 Evolution of the xenon signal after introduction of the gas in the NMR tube

The first series of experiments deals with single ^{129}Xe 1D spectra acquired after pulses of small flip angle at definite time intervals. Figure 3 displays typical examples of the evolution of the xenon intensity for two different solvents. In both cases, the xenon signal grows up in a first stage and then decreases. This is easily explained as resulting from dissolution combined with slow nuclear self-relaxation [4]. It can however be noticed that, in the case of CF_3CD_2OD (Fig. 3A), two clearly different time constants affect the decay of the xenon magnetization. Indeed the dotted line in Figure 3A corresponds to the best-fit theoretical curve with $k_{\rm diff} = 0$. In this condition, the reduced χ^2 rises from 0.60 (three exponential functions) to 4.26 (two exponential functions). A F-test reveals that the complete model ($k_{\rm diff} \neq 0$) is better with a probability higher than 99.999%. This clearly proves that three exponential functions are needed to describe the time dependence of the magnetization in the case of CF_3CD_2OD. According to our macroscopic model, the fast decay of xenon magnetization results from self-relaxation, while the slow decay corresponds to exchange between the solution and the gas phase which is, through the very long $T_1^{\rm g}$, a reservoir of polarized xenon. In contrast, for CD_2Cl_2 (Fig. 3B), it is impossible to separate these two contributions. We consequently use our macroscopic model to extract the dynamic parameters, either considering an explicit diffusion of xenon between the gaseous and liquid phases (three rates) or not (two rates). The results are summarized in Tables 1 and 2.

Considering the process of dissolution, *i.e.* the first stage where the signal is growing, two categories of solvent can be distinguished. For the first class illustrated in Figure 3A, which contains solvents such as benzene, cyclohexane, ... (Tabs. 1 and 2) but also for others (pyridine, dimethylsulfoxide) for which the signal to noise

Table 2. Dissolution rates k_{solv} and self-relaxation time T_1^{l} as extracted by fitting to equation (6), the time dependence of laser-polarized xenon signal without considering a diffusion constant k_{diff}. The proton dipolar contribution to relaxation $T_{1\mathrm{DD}}$ and its relative contribution %DD are extracted by comparing T_1^{l} values in non-deuterated and deuterated solvents and neglecting the ^{2}H dipolar contribution to xenon relaxation relative to the ^{1}H one. For non-deuterated pyridine, the signal to noise ratio is not sufficient to enable a reliable extraction of the rates.

Solvent	k_{solv} (min^{-1})	T_1^{l} (min)	$T_{1\mathrm{DD}}$ (min)	%DD
$C_6D_5CD_3$	1.76	17.5	-	-
$C_6H_5CH_3$		19.3		
CCl_4	3.6	22.5	-	-
$CDCl_3$	0.33	68.5	56.0	55
$CHCl_3$		30.8		
CD_2Cl_2	0.07	28.9	69.4	29
CH_2Cl_2		20.4		
C_5D_5N	0.12	18.5	-	-

ratios of the spectra are not sufficient to derive constant rates $(\lambda_1, \lambda_2, \lambda_3)$ with a high confidence, the dissolution step is very fast, k_{solv} is on the order of 1 min^{-1}. In contrast, for the second class illustrated in Figure 3B, which contains for instance chloroform, the dissolution step is very slow (k_{solv} on the order of 0.1 min^{-1}). This cannot simply be assigned to the difference in solubility of xenon, since it is almost identical in benzene and chloroform [26]. The correlation with the boiling point is also unclear. Hence the second class corresponds to solvents with a low boiling point, but benzene, cyclohexane, trifluoroethanol and tetrachloromethane, having almost the same boiling point (between 75 and 80 °C), exhibit a dissolution rate varying by a factor higher than 4.

Considering the relaxation step, not surprisingly the xenon signal remains observable for longer time when the solvent is deuterated than when it is in its natural form. From the difference between the decay rates of the signal, the ^{129}Xe–^{1}H dipolar relaxation times $T_{1\mathrm{DD}}$ between the dissolved gas nuclei and the solvent protons can be extracted. For this, we assume that the dissolution rate k_{solv} is identical in protonated and deuterated solvents (Tabs. 1 and 2). As illustrated by the trifluoroethanol family, the dipole-dipole contribution to relaxation for a given solvent seems to be directly related to the number of protons (difference 19% between CF_3CD_2OD and CF_3CD_2OH, 54% between CF_3CD_2OD and CF_3CH_2OH). The use of laser-polarized xenon should allow a better estimation of the xenon self-relaxation rates than with the classical inversion-recovery sequence. Indeed the latter method can easily be corrupted by the flow of excited xenon out of the detection coils, which leads to an apparent faster decay of the xenon magnetization and then to underestimation of T_1^{l}. The comparison should consequently be limited to measurements performed in conditions which take into account this effect. Our results for C_6H_6 and C_6H_{12} compare well with those of Navon *et al.* [4] or those of Moschos and Reisse [27] however performed at a different temperature.

A careful study of Table 2 (case of toluene) reveals that, even with laser-polarized xenon, the determination of the dipolar contribution to relaxation is delicate, when it is impossible to extract the contribution of diffusion between the gaseous and the liquid phase. This example illustrates how the coupling between these two phases can influence the dynamics of the xenon magnetization. This study represents also another example of the key importance of the coupling between transport phenomena and spin-relaxation processes (which depend on the local surrounding) when slow magnetization decay is present. Indeed the interpretation of the non-dipolar contribution to xenon relaxation in terms of spin-rotation, chemical shift anisotropy, ..., is impeded by the wide volume explored by xenon in a time scale on the order of T_1^{l}. This means that infrequent events inducing an efficient relaxation, as for instance paramagnetic relaxation resulting from elements present at the trace level, cannot be neglected.

3.3 Dissolution of xenon: a convective phenomenon

Whatever the solvent used, the signal of dissolved xenon appears surprisingly fast. Indeed, the average translational diffusion coefficient D measured in ^{1}H-NMR for the considered solvents is around 2×10^{-9} $\mathrm{m}^2\,\mathrm{s}^{-1}$ at ambient temperature, and we have checked that xenon dissolved in them adopts similar diffusion coefficients at equilibrium. The average displacement of xenon during a delay τ due to pure diffusion would be on the order of $\sqrt{D\tau}$. We consequently expect a displacement on the order of 0.2 mm in 30 s. Thus considering a distance of 10 mm between the gas/liquid interface and the detection coil, the observed dead-times t_0 (Fig. 3) are not at all compatible with a diffusive process, otherwise they would be on the order of hundreds of minutes. The fact that the xenon signal is observed in any solvent, even water, using our protocol (it is also present in the study of Navon *et al.* [4]) proves that convection occurs[3].

The convection phenomenon is not due to a permanent temperature gradient (which could result from heating of the bottom of the tube inherent to the temperature regulation system [29]), since, at equilibrium, the measured diffusion coefficients of benzene correspond to those reported in the literature. Moreover in experiments repeated at lower solvent temperatures, this effect continued to appear, which is not the signature of thermal convection.

As discussed in detail in Section 3.5, the requirement of two different parameters to describe the exchange between the gaseous and liquid phases (k_{diff} and k_{solv}) indicates a change in the transport mechanisms during the experiment. This proves that this convection exhibits a transient feature.

The convection cannot result from a temporary temperature gradient induced by the addition of gaseous

[3] For xenon dissolved in benzene, the diffusion coefficient values reported so far in the literature are higher by a factor about 5 [28], maybe due to this problem of convection in an experiment using laser-polarized gas.

xenon inside the tube **a**. Indeed, the convection appears whatever the initial temperature of the gas. Moreover the expansion does not produce a large cooling of the gas (a rough estimation leads to a gas temperature variation lower than 1 degree), and the heat capacity of about 3 mg of xenon is negligible with respect to that of the tube **a** (the overall mass of the tube with the liquid is ∼10 g). Also, the global cooling due to the solvation free enthalpy of xenon [30] is negligible (<0.01 degree). The convection cannot result from strong rf irradiations [31] which may induce local heating of the solution, since only low power pulses with small flip angles are used, and the effect is observed whatever the dielectric constant of the liquid. Furthermore, we have checked that the ^{129}Xe chemical shift, which strongly depends on temperature, does not vary from one spectrum to the next. In summary, this transient convection is mainly driven by gradient of xenon concentration and not of temperature. This gradient of concentration is coupled to the gravity field, since the magnetic force induced by the nuclear xenon magnetization in the presence of the magnet gradient is negligible ($\sim 10^{-8}$ N). This was experimentally checked by varying the sign of the xenon magnetization (sense of the polarization chosen during the optical pumping) and its amplitude (use of enriched xenon).

From a qualitative point of view, this convection effect is independent of the solubility of the gas in the considered liquid, as for example it is observed both in benzene (concentration of dissolved xenon = 0.14 M/atm at 290 K) and DMSO (0.024 M/atm at 298 K). As benzene and cyclohexane present different viscosities, this property also cannot be responsible of the convective effect. It is also not a question of density, as the same effect is observed for dissolution of xenon in trifluoroethanol, which has a density of 1.39 g/ml and in benzene (density 0.88 g/ml).

The size of our probehead does not allow us to vary on a large scale the sample geometry in order to see its influence on the convection process [32]. We have, however, tried to reduce the Rayleigh number by using NMR tubes of different inner diameter (4.2 mm, 3.5 mm and 2.2 mm) while keeping the same distance between the interface and the detecting coil. In all cases, the NMR signal of xenon dissolved in benzene appears but with a longer dead time t_0 when the inner diameter of the tube decreases. This proves that our limited range of Rayleigh numbers is already sufficient to observe an influence on the convection phenomenon in the expected direction.

3.4 Velocimetry experiments

In order to help understanding this convective phenomenon, we have performed dynamic imaging of the xenon flow inside the solvent. The results presented here correspond to measurements performed on deuterated benzene; similar results were also obtained in deuterated cyclohexane. The dissolution is so fast that it was impossible to simultaneously map the xenon diffusion along the three directions. We consequently acquired successive 1D or 2D

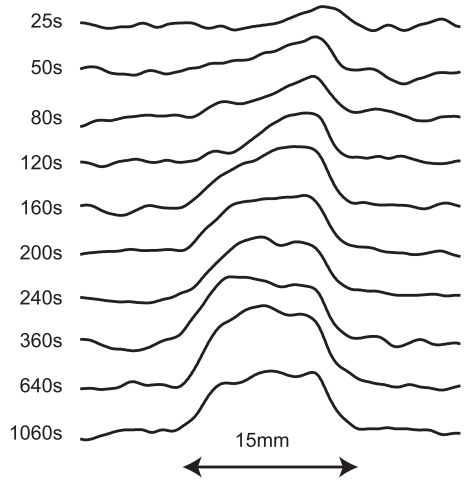

Fig. 4. Variation of the z profile of xenon dissolved in deuterated benzene as a function of time t.

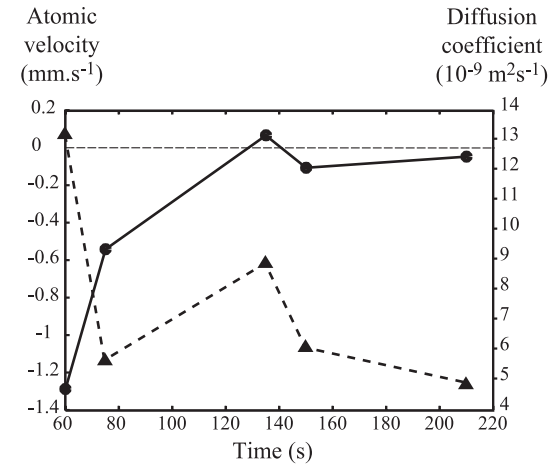

Fig. 5. Example of the evolution of the flux velocity (ordinates on the left side, solid line and plain circles) and of the diffusion coefficient (ordinates on the right side, dashed line and triangles) – both along z – as a function of time, during the first minutes after adding gaseous xenon in a degassed NMR tube containing a C_6D_6 solution. The abscissa indicates the time in seconds after the Joule – Gay Lussac expansion.

experiments allowing a qualitative description of the different features of the dissolution process.

The first experiment consists of monitoring the z profile of the xenon magnetization inside the solution as a function of time using small flip angles and z-gradient during acquisition. In agreement with what has been deduced previously, the xenon front moves towards the bottom of the tube by typically a few millimeters between each spectrum (interscan delay 30 s). The profile becomes almost flat in about 3 min (Fig. 4). In contrast to previous observations [4], we do not observe the accumulation of polarized xenon from the bottom of the tube.

The second series of experiments consists of time-resolved velocity and diffusion measurements of xenon displacement along the vertical (z) axis of the NMR tube. Figure 5 displays the evolution of the xenon velocity and

diffusion coefficient along z during the first steps of the dissolution of the gas in C_6D_6 in a z slice along a transverse axis[4]. The group velocity as well as the apparent diffusion coefficient are strongly time dependent, and are correlated to each other. The velocity measured 60 s after the mixing is very high (1.3×10^{-3} m s^{-1}), but much smaller than the sound speed in liquid, leading to very small Mach number [32]. Its decay is rather rapid and seems to oscillate around 0. For instance, 130 s after the mixing, the xenon velocity is positive, meaning that the global average displacement of magnetization, at this transverse coordinate, is towards the top of the tube. According to the measured velocities and the deduced distance covered by xenon, this should result from the upward flow required for mass conservation, which corresponds to xenon that has reached the bottom of the tube. This observation (in this particular experiment but also in others) is a signature of the presence of inhomogeneous xenon concentration inside the solution two minutes after adding the gaseous xenon, a result in agreement with the non flat z profile as observed in Figure 4. A similar decay appears for the diffusion coefficient, with also an oscillation 130 s after the mixing. The increase of the apparent diffusion coefficient for the initial times and the absence of simple evolution is also a clear indication of a convective process. After 6 min, the diffusion coefficient converges to its equilibrium value, while the group velocity vanishes. This result substantiates the previous conclusion of a transient convective phenomenon.

The final series of experiments are 2D time-resolved images of xenon inside the NMR tube obtained *via* a FLASH sequence [24,25]. A longitudinal image (xz-representation) is obtained after projection along y, a transverse image (xy-representation) is obtained after selection of an horizontal slice of 5 mm. In the case of longitudinal projection (Fig. 6), the fast arrival of xenon inside the tube is observed, with maximal xenon signal near the tube wall, giving a "$\bigcap$" shape. The preference of xenon for the edge of the tube is also observed in the transverse image (Fig. 7), where the typical xenon profile appears as a ring inside the cylindrical NMR tube. An edge-enhancement effect due to diffusion (see for example Ref. [33], or for gaseous laser-polarized xenon, Ref. [22]) cannot be responsible for the marked contrast in the images of Figure 7, since even considering the largest experimental diffusion coefficients (Fig. 5), the length scale associated with the encoding gradients $l_g = \sqrt[3]{D/\gamma G} = 20$ μm should give a less important effect [34] than observed. Moreover, the maxima of xenon intensity do not correspond to the wall of the NMR tube as expected from artifacts resulting from edge-enhancement by diffusion. Since xenon seems to flow towards the bottom of the tube preferentially along the glass wall, mass conservation implies that it must use the center of the tube for the reverse vertical travel. This has however never been observed.

[4] The impossibility of performing a complete 2D mapping in a very short time relative to $1/k_{solv}$ forbids the observation of the flow direction and amplitude in each voxel: only the average in the direction perpendicular to the read gradient is accessible.

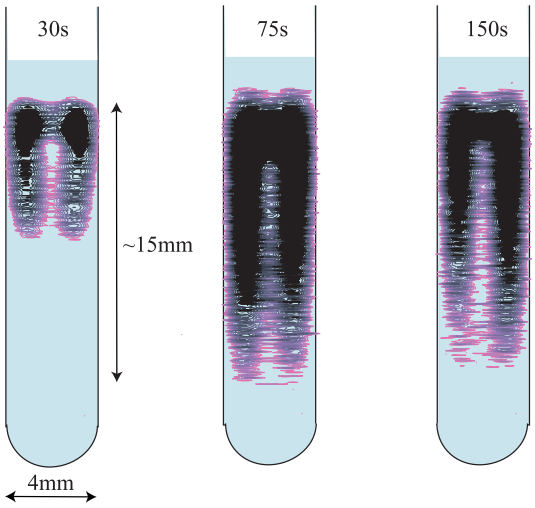

Fig. 6. Longitudinal images of the dissolution of gaseous xenon in C_6D_6 obtained by the FLASH sequence. Experimental conditions: 32 gradient values in the ramps from -25×10^{-3} to 25×10^{-3} Tm^{-1}.

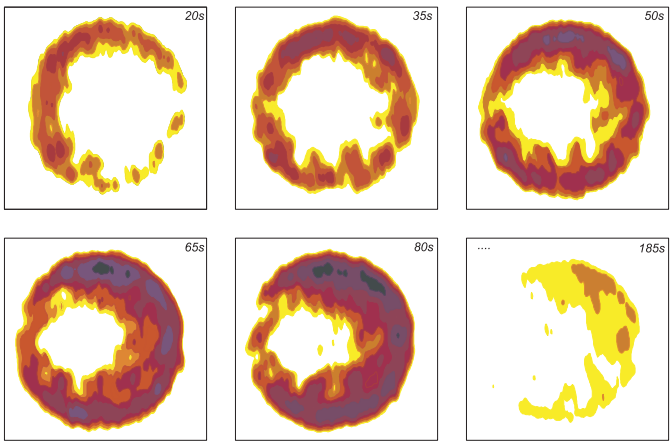

Fig. 7. Slice selected transverse images of the dissolution of gaseous xenon in C_6D_6 obtained by the FLASH sequence. Experimental conditions: slice selection obtained by combining a gradient pulse with a soft pulse of sinc shape (7 lobes) and duration 20 ms. 16 gradient values in the ramps from -25×10^{-3} to 25×10^{-3} Tm^{-1}.

The profile of this convection is different from first order static thermal convection previously observed in NMR tubes [31], as well as from buoyancy-driven convection (temperature-dependent fluid density) or convection due to surface tension gradients (temperature variations across the fluid surface) [35].

3.5 Macroscopic model and transient convection

In the light of this transient convection, it seems important to discuss the physical parameters used in our macroscopic model. Two physical mechanisms should be present: solvation of the gaseous xenon followed by its migration towards the detection coil. This can be expressed under the form of a xenon flow balance through a transverse

surface **S**. At the beginning, there is more xenon above than below the surface **S**: the xenon flow is directed from top to bottom whatever the transport mechanism. This mass transfer is efficient due to the presence of the transient convection and of the larger concentration of dissolved xenon above the solution. After about three minutes, as seen in the velocimetry experiments and confirmed by the study of the z profile of xenon (Fig. 4), the concentration of xenon is homogeneous and the transient convection phenomenon disappears. Still considering a flow balance through the surface **S**, the transport mechanisms have changed to an almost purely diffusive regime (as measured by comparative ^{1}H- and ^{129}Xe-diffusion experiments on benzene). The low efficiency of diffusion means that xenon detected by the NMR coil, *i.e.* well below the interface, now relaxes almost independently of gaseous xenon. This is effectively what is observed when one tries to fit different domains of the z profile of xenon as a function of time, since the extracted $T_1^{\rm l}$ are similar. However, as noticed in Figure 4 for long delay t, the magnetization at the bottom of the tube is smaller than at the top, an effect arising from the lower efficiency to renew xenon through diffusion when the distance to the interface increases.

The existence of these two mechanisms of mass transport as a function of time explains *a posteriori* the use of two different parameters $k_{\rm diff}$ and $k_{\rm solv}$ for describing the exchange processes between the liquid and gaseous phases. $k_{\rm solv}$ represents the transient convective process leading quickly to concentration equilibrium, while $k_{\rm diff}$ can be associated to the time-independent transport mechanisms which couple the gaseous and liquid phases[5]. However, it is obviously impossible to prove experimentally that the $T_1^{\rm l}$ extracted with non-zero $k_{\rm diff}$ values effectively correspond to real T_1, as defined in relaxation theory. Indeed this would require the complete vanishing of every transport mechanism altering the xenon concentration on time scale on the order of $5\,T_1^{\rm l}$, *i.e.* tens of minutes. The poor knowledge on this transient convection also precludes the use of more realistic models to treat the data.

In the absence of precise model, we have decided to perform crude simulations based on the available knowledge. Our aim is to reproduce data as those of Figures 3A and 4 or, at least, to give an understandable picture of the observed evolution of magnetization. For this, the dissolution process is treated as an exchange at the interface, characterized by an equilibrium constant and exchange rates, the transport mechanisms in solution being diffusion and convection. We assume a mono-exponential decay for the efficiency of the transient convection and derive its initial amplitude and decay constant from data of Figure 5. The nuclear spin self-relaxation rates of the dissolved and gaseous xenon are chosen according to the experimental measurements. The one-dimensional transport equation is numerically integrated using the mass conservation for each sample slice. The increment time used in the simulation is chosen for stability on the order of 1 ms. This numerical integration is carried out simultaneously on polarized and non-polarized xenon.

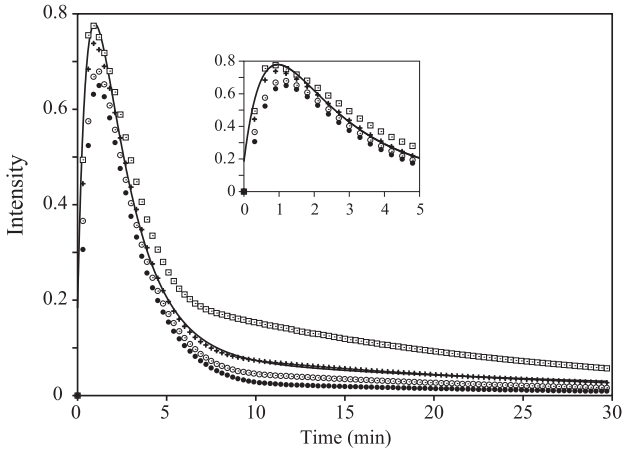

Fig. 8. Example of the time dependence of xenon magnetization obtained by numerical simulations, assuming $T_1^{\rm l} = 120$ s. The crosses correspond to the global magnetization detected by the coil. The solid line is the best-fit theoretical curve to equation (6). The open squares, open circles and filled circles correspond to the magnetization in z-slices at 10, 20 and 25 mm below the interface, respectively.

In Figure 8 the simulated xenon magnetization at three locations (10 mm, 20 mm and 25 mm below the interface) and the global magnetization detected by the coil are represented. The simulated curves exhibit behaviors similar to the experimental ones (Fig. 4): the distance from the interface defines the rate of magnetization build-up as well as of its decay. The time dependence of the global magnetization detected agrees well with the macroscopic model (Eq. (6)), and the extracted $T_1^{\rm l}$ corresponds to the simulated one at a level better than 1%. By varying the parameters in the simulation, it appears that, when $k_{\rm diff}$ can be precisely extracted, the determined $T_1^{\rm l}$ agrees with the one used in the simulation at a level better than typically 5%. This gives a rough estimation of the accuracy of the self-relaxation times given in Table 1.

The simulation actually reveals that when $k_{\rm diff}$ cannot be determined, the best-fit $T_1^{\rm l}$ value is larger than the one used in the simulation. This effect is undoubdly responsible of the much longer $T_1^{\rm l}$ found for the solvents of Table 2 and for the non realistic values of $T_1^{\rm l}$ in the case of deuterated or non-deuterated toluene. This result can be physically interpreted using the flow balance through the surface **S**: the retrodiffusion from the dissolved xenon to the gaseous phase cannot be distinguished from the dissolution step in term of transport mechanisms. As a consequence, the decay of dissolved polarized xenon due to spin relaxation can be compensated by transport of polarized xenon from the gaseous phase, leading to long apparent $T_1^{\rm l}$. Probably this apparent $T_1^{\rm l}$ has no physical meaning in term of spin relaxation, but it characterizes well the typical duration of an experiment which can use laser-polarized dissolved xenon in these solvents.

[5] In fact, equation (3) can be reinterpreted in term of a simple exchange between gaseous and dissolved xenon which rate is monoexponentially decaying as a function of time towards $k_{\rm diff}$.

4 Conclusion

The dissolution of laser polarized xenon at pressures on the order of one atmosphere in degassed liquids appears to be a transient convective process allowing the homogenization of the xenon concentration in solution in a few minutes. This convection, which does not result from a temperature gradient, is present in each liquid we have studied, even those, such as water, where the solubility of xenon is very low. Thus the first dissolution step of xenon differs strongly from the process of liquid/gas exchange at equilibrium, since the latter is found to be mainly diffusive, as in the case of CO [36]. For this transient convective process, xenon flows down with the solution along the wall. The present study based on laser-polarized xenon and MRI techniques allows a first quantitative characterization of this phenomenon. We note that the constraints imposed by the geometry of a liquid-state probehead seem to forbid a better characterization, *e.g.* a higher time-sampling rate, change of sample symmetry, large variation of the Rayleigh number, significant change of the delivery process or of the xenon pressure. A finer description of this transient process by more classical optical procedure [37] would then be necessary. Nevertheless, the appearance of convection induced by concentration gradient could limit the use of fast MRI techniques. Indeed, although the dissolved xenon diffusion length at concentration equilibrium is much smaller than the resolution of the magnetic resonance image, dephasing of spins due to convective diffusion during application of imaging gradients could result in a substantial loss of signal [28].

The dynamics of laser-polarized xenon magnetization is strongly dependent on the solvent, since for a particular solvent such as chloroform, the dissolved-phase spin relaxation is slowed down by an efficient mass transfer process between the dissolved xenon and the reservoir of slow-relaxing gaseous xenon, leading to a very long apparent self-relaxation time T_1^{l}. The present result, which illustrates how global transport phenomena and local dynamic properties such as spin relaxation can be mixed, has important consequences for the ideal delivery process in continuous flow laser-polarized xenon experiments. For example, for a solvent such as chloroform, it could be better to avoid spectrum artifacts resulting from bubbling the gas in the solution, and to benefit from the strong coupling between the gaseous and liquid phases, by adding freshly polarized xenon gas above the solution and not inside.

We would like to thank Luc Belloni, Pierre Carlier, François Daviaud, Anne Leroy and Claire Wary for helpful discussions. Financial support from French Ministery of Research is acknowledged (ACI #4103).

References

1. M.A. Bouchiat, T.R. Carver, C.M. Varnum, Phys. Rev. Lett. **5**, 373 (1960)
2. G.D. Cates, D.R. Benton, M. Gatzke, W. Happer, K.C. Hasson, N.R. Newbury, Phys. Rev. Lett. **66**, 2591 (1990)
3. M. Gatzke, G.D. Cates, B. Driehuys, D. Fox, W. Happer, B. Saam, Phys. Rev. Lett. **70**, 690 (1993)
4. G. Navon, Y.-Q. Song, T. Rõõm, S. Appelt, R.E. Taylor, A. Pines, Science **271**, 1848 (1996)
5. Y.-Q. Song, B.M. Goodson, R.E. Taylor, D.D. Laws, G. Navon, A. Pines, Angew. Chem. **36**, 2368 (1997)
6. M. Lühmer, B.M. Goodson, Y.-Q. Song, D.D. Laws, L. Kaiser, M.C. Cyrier, A. Pines, J. Am. Chem. Soc. **121**, 3502 (1999)
7. H. Desvaux, T. Gautier, G. Le Goff, M. Pétro, P. Berthault, Eur. Phys. J. D **12**, 289 (2000)
8. C. Landon, P. Berthault, F. Vovelle, H. Desvaux, Prot. Sci. **10**, 762 (2001)
9. P. Berthault, C. Landon, F. Vovelle, H. Desvaux, C. R. Acad. Sci. Ser. IV **2**, 327 (2001)
10. S. Appelt, F.W. Haesing, S. Baer-Lang, N.J. Shah, B. Blümich, Chem. Phys. Lett. **348**, 263 (2001)
11. R.J. Fitzgerald, K.L. Sauer, W. Happer, Chem. Phys. Lett. **284**, 87 (1998)
12. M. Haake, B.M. Goodson, D.D. Laws, E. Brunner, M.C. Cyrier, R.H. Havlin, A. Pines, Chem. Phys. Lett. **292**, 686 (1998)
13. J.C. Leawoods, B.T. Saam, M.S. Conradi, Chem. Phys. Lett. **327**, 359 (2000)
14. M. Haake, A. Pines, J.A. Reimer, R. Seydoux, J. Am. Chem. Soc. **119**, 11711 (1997)
15. R. Seydoux, A. Pines, M. Haake, J.A. Reimer, J. Phys. Chem. B **103**, 4629 (1999)
16. E. MacNamara, G. Fisher, J. Smith, C.V. Rice, S.-J. Hwang, D. Raftery, J. Phys. Chem. B **103**, 1158 (1999)
17. I.L. Moudrakovski, S. Lang, C.I. Ratcliffe, B. Simard, G. Santyr, J.A. Ripmeester, J. Magn. Reson. **144**, 372 (2000)
18. T.G. Walker, W. Happer, Rev. Mod. Phys. **69**, 629 (1997)
19. P. Berthault, H. Desvaux, G. Le Goff, M. Pétro, Chem. Phys. Lett. **314**, 52 (1999)
20. P. Mansfield, I.L. Pykett, J. Magn. Reson. **29**, 355 (1978)
21. P.T. Callaghan, Y. Xia, J. Magn. Reson. **91**, 326 (1991)
22. Y.-Q. Song, B.M. Goodson, B. Sheridan, T.M. de Swiet, A. Pines, J. Chem. Phys. **108**, 6233 (1998)
23. R.W. Mair, C.H. Tseng, G.P. Wong, D.G. Cory, R.L. Walsworth, Phys. Rev. E **61**, 2741 (2000)
24. A. Haase, J. Frahm, D. Matthaei, W. Hänicke, K.-D. Merboldt, J. Magn. Reson. **67**, 258 (1986)
25. M. Rokitta, U. Zimmermann, A. Haase, J. Magn. Reson. **137**, 29 (1999)
26. H.L. Clever, *IUPAC solubility data series* (Pergamon Press, Oxford, 1979)
27. A. Moschos, J. Reisse, J. Magn. Reson. **95**, 603 (1991)
28. J. Wolber, S.J. Doran, M.O. Leach, A. Bifone, Chem. Phys. Lett. **296**, 391 (1998)
29. N. Hedin, I. Furó, J. Magn. Reson. **131**, 126 (1998)
30. A. Ben-Naim, *Solvation thermodynamics* (Plenum Press, New York, 1987)
31. A. Jerschow, J. Magn. Reson. **145**, 125 (2000)
32. F. Kreith, *Fluid mechanics* (CRC Press, Boca Raton, 2000)
33. P.T. Callaghan, A. Coy, L.C. Forde, C.J. Rofe, J. Magn. Reson. A **101**, 347 (1993)
34. T.M. De Swiet, J. Magn. Reson. B **109**, 12 (1995)
35. S.J. Gibbs, T.A. Carpenter, L.D. Hall, J. Magn. Reson. A **105**, 209 (1993)
36. N. Aebischer, R. Churlaud, L. Dolci, U. Frey, A.E. Merbach, Inorg. Chem. **37**, 5915 (1998)
37. M. Raffel, C.E. Willert, J. Kompenhans, *Particle image velocimetry a practical guide. Experimental fluid mechanics* (Springer, Berlin, 1998)